Easy repair enabled by an interleaving ‘weak link’ strategy to localise damage in laminated fibre-reinforced polymer-matrix composites

Bohao Zhang[1], Gokul G. Murali[1], Tomás Francisco Hut Quitéria[1], Jakub Porzycki[1], Yibo Bai[1], Daniel Liew[1], Tianyou Deng[1], Chun Hei Yu[1], Sameer Kanneganti[1], Christroph Burgstaller[2], Alexander Bismarck[3,4] and Paul Robinson[1*]

[1] The Composites Centre, Department of Aeronautics, Imperial College London, South Kensington Campus, London SW7 2AZ, UK

[2] Transfercenter für Kunststofftechnik (TCKT), Franz-Fritsch-Straße 11, A-4600, Wels, Austria

[3] Polymer and Composite Engineering (PaCE) group, Institute of Materials Chemistry and Research, University of Vienna, Währinger Strasse 42, A-1090 Wien, Austria

[4] Department of Chemical Engineering, Imperial College London, South Kensington Campus, London SW7 2AZ, UK

Keywords: Carbon fibres, Hybrid composites, Multifunctional composites, Strength, Structural composites, Repair

Abstract

An interleaving strategy for polymer matrix composite laminates is proposed to create a mechanical fuse allowing interlaminar damage to be localised in the interleaf, which can subsequently be repaired. To create the mechanical fuse, the laminates are interleaved with thermoplastic polymer films with suitable mechanical properties to act as a repairable weak link. Carbon fibre/epoxy laminates interleaved with polystyrene (PS) were investigated by three-point flexure and static indentation tests. In the three-point

---

[*] Corresponding author: phone: +442075945073; e-mail: p.robinson@imperial.ac.uk

bending tests, shear–driven damage was observed in the interleaved region, and this damage was subsequently repaired by application of heat and pressure. After two damage-repair cycles, the stiffness was virtually fully recovered, and the shear strength restored to 88% of the pristine value. In the static indentation tests, the stiffness and damage onset force of the specimens recovered to 84% and 70% of the pristine values, respectively, after three damage-repair cycles.

1 Introduction

Laminated fibre-reinforced polymer composites with high specific strength and stiffness are attractive materials for weight-sensitive applications in the aerospace, automotive, and wind energy sectors. However, due to the relatively low strength of the polymer matrix, these materials are vulnerable to interlaminar damage. Such damage, for example, due to impact, can significantly compromise the structural integrity of composites, particularly in compression [1]. A common method to restore the structural integrity with a flush or near-flush surface appearance is to remove the damaged material by machining, usually at a shallow angle, and then to adhesively bond a repair patch in its place [2-4]. Alternatively, the damaged area may be repaired by drilling a hole in the centre of the damaged section and then injecting liquid resin, which is subsequently cured [5-7]. Unfortunately, such repair techniques are time-consuming, expensive and require considerable skill and experience to achieve consistently high-quality repairs. For these reasons, 'self-healing' composites have attracted considerable interest [8, 9]. Such composites often contain microcapsules filled with a healing resin and hardener, stored separately within the composite matrix [10-15]. Provided the damage process ruptures the microcapsules dispersed within the composite, causing the hardener and resin to seep into the cracks and mix, then some degree of repair can be achieved. For example, in tapered double cantilever specimens, which were allowed to self-repair at room temperature, an average recovery of 60% in fracture force was measured [15]. It is also possible to use microcapsules containing a single-component adhesive, such as cyanoacrylates [16, 17]. The effectiveness of the repair achieved with microcapsule systems is often limited by the quantity of healing agent available and by the shelf life of the healing agent due to ageing effects. To address this issue, vascular architectures consisting of a network of hollow glass fibres embedded within the composite have been proposed [18-27]. (Alternatively, a vascular system can be created within the resin matrix by including, prior to cure, wires of a suitable material which, after curing, can be removed [23, 24].) Using this vascular architecture, resin in sufficient quantities can be transported to the damage site either by capillary forces [22] or by pumping [20] resulting in effective repair. Although the microcapsule and vascular 'self-healing' approaches do avoid the drawbacks of traditional repair strategies, the incorporation of such systems within the composite inevitably introduces additional complications during manufacturing, particularly for vascular systems, and can reduce the stiffness and strength of composite parts [13, 25]. Damaged areas in composites containing embedded microcapsules can only be healed once, but subsequent healing at the same position is not possible [19, 21]. In contrast, multiple healing cycles of composites containing vascular networks are possible but the healing efficiency is reduced significantly to 50% after 10 repeated damage-repair cycles [20].

A matrix material, which can be readily repaired by thermal treatment, has also been proposed. Chen *et al.* [28, 29] proposed a mendable matrix system formed by multi-diene and multi-dienophile monomers, which undergo Diels-Alder cycloaddition on heating. Hayes *et al.* [30, 31] investigated a different mendable matrix approach; they manufactured a glass-fibre reinforced composite system with a matrix blend consisting of an epoxy resin with methyl-5-norbornene-2,3-dicarboxylic anhydride hardener and a thermoplastic poly(bisphenol A-co-epichlorohydrin) healing agent, which was dissolved in the epoxy resin at 80°C. Specimens of this mendable matrix material were impacted, then heated to 160°C for 1 h under an applied pressure of 0.2 MPa and re-impacted. The results showed that 65% of the initial impact strength could be recovered but strength recovery significantly decreased to around 35% after three impact-healing cycles. Pingkarawat *et al.* [32, 33] developed a composite laminate containing mendable poly (ethylene-co-methacrylic acid) (PEMAA) particles dispersed throughout the matrix or 2-4 layers of PEMAA fibre meshes in the mid-plane. Double cantilever beam (DCB) tests were performed on these composites and heated afterwards to 150°C for 30 mins, followed by re-testing to determine the healing effectiveness. The mode I fracture toughness after the first healing cycle exceeded that of the control specimens (not containing PEMAA fibre meshes) by more than 200%. However, subsequent repeated healing resulted in a reduced repair efficiency due to the depletion of functional groups in PEMAA available to re-bond the fracture surface. Amael *et al.* [34, 35] developed a 'self-healing' matrix consisting of a blend of diglycidyl ether bisphenol A (DGEBA) epoxy resin with 4,4'-diaminodiphenylsulfone hardener and poly(ε-caprolactone) (PCL) and manufactured glass fibre reinforced composites using this matrix. These composites were subjected to DCB tests, then exposed to 150°C for 30 mins under a compressive load of 50 kPa normal to the surface to heal the interlaminar crack followed by re-testing. Three damage-repair cycles were performed to evaluate the repair efficiency. The recovered fracture toughness of the specimens after three cycles was between 40% to 60% of the initial value of pristine composites. Kandemir *et al.* [36] reported the repair performance of aligned, discontinuous flax fibre vitrimer resin composites. Specimens of the material was tested in tension, then the broken specimens were heated at 120°C in a semi-closed mould with an applied pressure of 0.69 MPa for 5 mins, followed by re-testing. Test results showed that the tensile strength of the specimens were recovered by an average of 36%. Palubiski *et al.* [37] examined the repairability of multi-matrix composite systems in which vitrimer resin was incorporated in the region susceptible to interlaminar damage. Four-point bending test results of a corner specimen showed that the strength recovery after one test-repair cycle was 233% and after two cycles 118%. For these tests, the specimens were repaired by heating in an oven at 110°C under vacuum pressure for 2 h. The increase in strength after the first repair was speculated to be due to an improved vitrimer performance because the repair time significantly exceeded the initial curing duration and that defects in the specimens caused by the cutting process may have been healed during the first repair process.

In our research reported in this paper, we have explored the use of polymer interleaves to create a repairable composite. Polymer interleaves have been previously exploited to improve the toughness of fibre-reinforced polymer matrix composites. It has been reported that interlaminar fracture toughness can be significantly improved [38-40], and the initiation of impact damage can be suppressed by suitable interleaves [41]. Some work explored the use of interleaves for composite repair. Thorn *et al.* [42] investigated the repair performance of carbon fibre/epoxy composite interleaved with phenoxy films subjected to double cantilever beam (DCB) tests. After the initial tests, specimens were repaired by preheating for 10 mins in a hot press at 180°C followed by pressing the specimens for 2 mins at 50 bar. The recovery of the peak force and interlaminar propagation toughness were 99% and 34%, respectively, which dropped after one test-repair cycle to 62% and 26% after four test-repair cycles. In a further study on phenoxy interleaves, separated strips of phenoxy running across the width of the midplane of carbon fibre-epoxy DCB specimen were investigated for two grades of phenoxy with different molecular weights [43]. The highest toughness after one test-repair cycle (following the repair process [42]) was obtained with 5 mm wide interleaf strips of the lower molecular weight phenoxy separated by 5 mm. For these specimens, the recovery of peak force and interlaminar propagation toughness were 84% and 77%, respectively, but the authors noted that there was very significant stick-slip behaviour due to the discontinuous interleaf. OuYang *et al.* [44] reported a carbon fibre/epoxy $[(+\theta/-\theta)_2]_s$ composite interleaved with a hierarchical CNT/EP/EMAA interleaf at the $+\theta/-\theta$ interfaces. Specimens were tested in tension to generate edge delamination and then repaired by electrical Joule heating of the CNT/EP layers to 150°C for 1 h. Interleaved specimens with θ = 20° and θ = 30° achieved high healing efficiencies with recoveries of the delamination initiation stress of 107% and 99%, respectively, after two delamination-repair cycles.

It is evident from the literature that interleaving with suitable polymers at the location of the anticipated interlaminar failure has the potential to achieve high repair efficiencies. We explore the possibility of ensuring that failure occurs only in the interleaf location, thereby facilitating an effective and easy repair. Extending previous work, we propose a 'weak link' concept using thermoplastic interleaves to enable easy, and repeatable repair of shear-driven interlaminar damage [45]. Interlaminar damage in polystyrene-interleaved carbon fibre-epoxy composites was induced by three-point bending and static indentation tests. The damaged specimens were repaired and re-tested to evaluate stiffness and strength recovery and the process was repeated to demonstrate any degradation with further damage-repair cycles. (Studies using two other interleaf materials to demonstrate the limitations of the concept are described in the supplementary material.)

2 The weak link interleaf concept

In mechanical systems, shear pins are often used as a weak link or mechanical fuse. Shear pins are replaceable sacrificial elements designed to fail preferentially in the event of an overload condition to protect other parts that are more difficult and/or expensive to repair or replace. For a composite laminate, it is impossible to introduce an element, which can be readily replaced in case of damage. Instead, a simple repairable weak link in the form of a thermally bondable interleaf with a shear strength lower than that of the fibre-reinforced matrix could be incorporated into composite laminates. Provided that a sufficiently strong interface exists between the interleaf and the matrix, then shear-driven interlaminar damage will preferentially occur within the interleaf region of composite laminates when loaded. Such damage can be repaired by application of heat and pressure, similar to the mendable matrix systems discussed earlier.

Fig. 1 illustrates the damage-repair cycle of the proposed weak-link interleaved composites. On impact, interleaved composites should preferentially fail within the interleaf layer, assuming the impact energy is not so high as to cause in-plane failure of the plies due to bending/membrane stresses. To repair the damaged laminated composite, it has to be heated and subjected to external pressure to trigger the restoration of an intact interleaf. Therefore, a suitable interleaf material will have to possess the following characteristics:

i) Have a shear strength lower than the interlaminar shear strength (ILSS) of the parent composite laminate (so that the interleaf does act as a weak link) but not so low that the interleaved composite becomes too susceptible to interlaminar damage.

ii) Be capable of thermal bonding to itself at a temperature, which will not degrade the parent composite laminate.

iii) Be able to withstand the cure conditions of the parent composite and to remain as a continuous, discrete layer in the cured composite.

iv) Possess a good bond strength to the matrix of the parent composite so that failure will occur within the interleaf.

An alternative approach is to use an interleaf which has an interfacial shear strength with the parent matrix which is lower than both the interlaminar shear strength of the composite and the shear strength of the interleaf. In this case, the shear-driven damage will occur preferentially at the composite-interleaf interface and to achieve a repair the interleaf must be capable of thermally re-bonding to the parent composite.

To demonstrate the concept that the selected interleaf does act as a 'weak link', short-beam shear tests were performed to assess the ILSS of non-interleaved and interleaved composite specimens. Three-point bending tests were performed on interleaved composite specimens to investigate whether a shear-driven failure does occur in the interleaved region (as required by the weak link approach), and that after repair, the stiffness and strength can be restored. Practical applicability is demonstrated using static indentation tests conducted to determine the extent to which the easy repair approach can restore the performance of the interleaved specimens following impact-like damage.

3 Experimental

3.1 Materials

TS300/914 carbon fibre/epoxy prepreg (Hexcel UK) was selected as the composite system, although it is equally applicable to other thermoset and even thermoplastic composites. TS300/914 has a curing temperature of 175°C, a nominal cured ply thickness of 125 μm and ILSS of 78 MPa, according to the manufacturer's datasheet [46]. Polystyrene (PS) (Empera 124N) was selected for the thermoplastic interleaf material as it possessed sufficiently low shear strength (15 MPa) to demonstrate the 'weak link' concept [47], a low enough glass transition temperature ($T_g \approx 100$°C) [48] and high enough processing temperature ($T_p \approx 200$°C) to enable easy repair by heating and film stability during composite manufacturing. (PS is not proposed to be the optimum interleaf material choice but was selected as a model material to demonstrate the weak link/easy repair concept.) Rolls of thin PS films (70 µm thick) were prepared by Transfercenter für Kunststofftechnik (TCKT, Austria). The material was produced by film extrusion using an extruder (Plastik Maschinenbau PM 30, Kelburg, Germany) equipped with a tapered screw (diameter: 30 mm, length: 102 cm) and a flat film die. The temperatures in the extruder varied depending on the intrinsic thermomechanical properties of the polymer. The screw speed was set at 58 rpm, which resulted in a melt pressure of ~120 bar. The take-off speed was ~5.1 m/min while the chill roll temperature was ~10°C.

3.2 Manufacturing composite test specimens

For the short-beam shear and three-point bending tests, composite panels (175 mm x 120 mm) consisting of 24 plies 0° carbon fibre/epoxy prepregs and an interleaf (IL) layer in a unidirectional layup configuration $[0°_{12}/IL/0°_{12}]$ were laid up. As control a non-interleaved, unidirectional carbon fibre/epoxy composite (CFRP) with a $[0°_{25}]$ layup was manufactured. For static indentation tests, interleaved composite panels (180 mm × 120 mm) in a quasi-isotropic configuration $[(0/IL/90/IL/{+45}/IL/{-45}/IL)_3/(IL/{-45}/IL/{+45}/IL/90/IL/0)_3]$ were laid up. The panels were cured at 175°C and 6.89 bar (100 psi) pressure in an autoclave for 1 h according to the prepreg manufacturer’s curing schedule. The cured panels were c-scanned to detect any defects introduced during manufacturing. Specimens used for short beam shear tests (nominally 15 mm × 6 mm), three-point bending tests (nominally 80 mm × 10 mm), and static indentation tests (nominally 150 mm × 100 mm) were cut from the cured panels. The measured dimensions of the specimens are reported in Table 1.

3.3 Short-beam shear test

Short-beam shear tests were conducted in accordance with ASTM D2344M. The specimens were loaded in a short-beam shear fixture in a universal test machine (Instron 5960 series, USA) equipped with a 50 kN load cell. A support span of 12 mm was used. The diameter of the support and loading rollers was 6.4 mm. The short-beam shear tests were conducted at a crosshead speed of 1 mm/min at room temperature until the specimens showed a significant loss in load. At least five specimens of each configuration (non-interleaved and interleaved) were tested.

The associated ILSS was calculated using:

$$\text{ILSS} = \frac{3 \cdot P_c}{4 \cdot t \cdot w} \quad (1)$$

where P_c is the measured failure load and w, t the specimen width and thickness.

The failure load P_c was taken as the load at which the compliance of the specimens increased by 1%. The initial compliance was measured within the mid-span displacement range of 0.15-0.20 mm for non-interleaved and 0.08-0.11 mm for PS interleaved composites. (The selected ranges were within the linear regimes of the recorded load-displacement plots.) This technique, which effectively determines the departure from linearity in the load-displacement curve, has been used to measure the shear strength of adhesives [49].

3.4 Three-point bending test

The flexural tests were performed in a three-point bending fixture according to ASTM D7264M. Each specimen was loaded in a universal test machine (Instron 5960 series, USA) equipped with a 50 kN load cell. A support span of 70 mm was chosen, based on the measured ILSS value of the interleaved specimen, to ensure that the specimens failed in interlaminar shear rather than flexure. The diameter of the support and loading rollers was 6 mm. The test was conducted at a constant crosshead speed of 1 mm/min at room temperature until the specimens showed a significant loss in load. At least five specimens of each interleaf material were initially tested.

The load associated with the onset of shear failure P_c was taken as the maximum load achieved in the test (the failure was abrupt and not progressive like the ILSS failure process). The associated shear strength τ^u was calculated using equation (1). It should be noted that equation (1) is not strictly applicable to the interleaved specimens, but the error is negligible (less than 0.1%) for the case of a thin mid-plane interleaf as used here.

3.5 Static indentation test

The static indentation tests were conducted according to ASTM D6264M on the test machine (Instron 5960 series, USA) equipped with a 50 kN load cell. The interleaved composite panels were clamped by a square steel support fixture of 250 mm with an indentation window 100 mm long and 65 mm wide. The support fixture was secured using four bolts, tightened to a torque of 10 Nm measured using a torque wrench. (This torque level ensured that there was no damage caused to the panels during mounting.) A hemispherical indenter of 12.7 mm in diameter was used. The pristine panels were indented at the centre point at a constant crosshead speed of 1.25 mm/min until a significant slope change in the force-displacement curves indicated onset of damage and loading continued to an applied displacement of approximately 1.1 mm to propagate the damage. (Subsequent c-scans showed that the damage zone was approximately 17.8 mm in diameter.) Repaired specimens were loaded to the same maximum displacement. The initial compliance was determined over the displacement range of 0.2-0.4 mm in the force-displacement plot, and the load associated with the damage onset was taken as the load at which the compliance of the specimens increased by 1%. Nine specimens were tested.

3.6 Characterisation of fracture surfaces

For the interleaved composites, which failed in the interleaf region in the three-point bending tests, characterisation of the fracture surfaces was performed to determine whether the failure occurred in the interleaf layer or at the interfaces between the interleaf and the carbon epoxy laminae. Failed specimens were separated into two halves (through the thickness), and both fracture surfaces were analysed by X-ray photoelectron spectroscopy (Nexsa X-Ray Photoelectron Spectrometer (XPS) System, ThermoFisher Scientific Inc., USA). Using the chemical composition of both fracture surfaces, the location of the failure was identified. Surfaces of cured non-interleaved composite short beam shear specimens and interleaf films were also analysed using XPS for comparison. The studied surfaces were initially cleaned using argon ion etch with an energy of 6000 eV for 60 s using Ar clusters of 1000 atoms. High-resolution XP spectra of carbon (C1s), nitrogen (N1s), and oxygen (O1s) were recorded using Al-K_{α} X-rays with a 400 µm size spot with 1 eV resolution.

3.7 Repair process

Each flexural specimen failed in the interleaf region and debonded into two halves. The two halves were stacked back together, using an engineers square and high-temperature resistant tape to ensure precise alignment. The specimen was then placed on the bed of a heated vacuum press (Global vacuum heat press, Nabuurs Developing S.L., Spain) covered with PTFE release films and breather cloth and finally covered with the rubber membrane of the vacuum press. The assembly was then subject to vacuum pressure of -0.9 bar and heated from room temperature to a repair temperature of 170°C. This temperature was chosen as it is sufficiently higher than T_g of PS, thus allowing interdiffusion of PS chains. The specimens were kept at this temperature for 5 mins, then cooled down to room temperature under applied vacuum. The repaired specimens were re-tested to determine the recovery of their shear strength. The specimens were subjected to two damage-repair cycles.

The static indentation specimens were c-scanned to determine the indentation damage region after testing, followed by repair at 170°C for 5 mins under pressure on the heated vacuum table. After the repair, they were re-c-scanned to examine whether the induced damage had been repaired. The specimens were re-tested to evaluate the recovery of the stiffness and damage onset force. Three damage-repair cycles were conducted.

3.8 <u>Optical microscope examination</u>

Polished cross-sections of composite specimens were inspected by optical microscopy (ZEISS Axio Imager 2, Carl Zeiss AG, Germany) after manufacture, failure, and subsequent repair. Composite sections were mounted in polyester potting resin and cured at room temperature. The mounted specimens were polished in a grinder-polishing machine (Saphir 550, ATM GmbH, Germany) using P600 SiC grinding paper followed by polishing using diamond (9 μm), alumina (0.6 μm) and silica (0.03 μm) dispersions before microscope examination.

4 Results and discussion

4.1 <u>Short beam shear tests</u>

Fig. 2 shows typical load-displacement curves from short beam shear tests of a non-interleaved specimen and a PS-interleaved specimen. The non-interleaved specimen failed suddenly at around 2400 N but failure was preceded by a departure from linearity at around 1600 N. Based on departure from linearity (see section 3.3), the average ILSS of the non-interleaved composites was determined to be 67.5 MPa (Table 2). Microscope examination of a non-interleaved specimen (Fig. 3a) shows that delamination occurred due to shear above the mid-plane of the specimen.

A typical load-displacement curve of a PS-interleaved specimen is shown in Fig. 2 indicating that the PS-interleaved specimen started to yield at around 700 N (due to shear yielding of the PS interleaf), followed by failure at around 2000 N. The average ILSS of the PS-interleaved specimens corresponding to the yielding onset point was 31.3 MPa (Table 2) much lower than the ILSS of the non-interleaved composite as required for the 'weak link' concept. The shift of the interlaminar failure to the mid-plane confirms that the PS interleaf does indeed act as a weak link (see Fig. 3).

4.2 Three-point bending tests

Typical load-displacement curves of a PS–interleaved specimen in the pristine state, after the first repair and after the second repair are shown in Fig. 4. The stiffnesses of the specimen after the first repair and second repair were in good agreement with that of the pristine specimens. The average shear strength of the pristine PS-interleaved specimens was 27.3 MPa and after two damage-repair cycles, the average shear strength slightly reduced to 23.9 MPa (87.9% of pristine value – see Table 2). (The shear strength determined from the three-point bending tests of the pristine PS-interleaved specimens was lower than the ILSS value from the short beam shear tests but it should be noted that the short beam shear test is widely regarded as a qualitative rather than a quantitative method [50, 51].)

All PS-interleaved specimens failed in the interleaf region due to shear. A typical fracture surface of a failed pristine PS interleaved composite showing evidence of a very thin PS layer present on both fracture surfaces is shown in Fig. 5. An optical microscope image of the longitudinal cross-section of a pristine interleaved specimen (Fig. 6a) shows that a distinct continuous PS layer between composite plies was achieved. After a three-point bending test, the damage appears to be at the upper side of the PS interleaf but no damage within the composite plies can be seen (Fig. 6b). Upon application of pressure and temperature, the PS interleaf region was repaired (Fig. 6c) but afterwards this region is thinner than the in the pristine case because some PS was squeezed out from the specimen edges (Fig. 6d) during the repair.

To verify whether failure of the interleafed composite occurred cohesively within the PS interlayer XPS spectra were recorded. Fig. 7 shows the carbon (C1s), oxygen (O1s) and nitrogen (N1s) high-resolution XP-spectra of the surface of a non-interleaved composite specimen, of PS film, and of the fracture surfaces of a PS-interleaved composite flexure test specimen. The atomic compositions are summarised in Table 3. Deconvolution of the C1s spectra of the fracture surface of a non-interleaved composite specimen confirmed the presence of C-C and C=C peaks (~284 eV), C-O peaks (~285.5 eV), and C=O peaks (~287.5 eV) as expected for a cured epoxy matrix. The deconvoluted C1s spectra of PS are similar to those reported for PS in the literature [52]. The high-resolution C1s XP spectra of the two fracture surfaces show the presence of peaks associated with π-π* interactions (~291 eV), characteristic for PS, that were not present in spectra of the control composite, indicating that a thin PS layer indeed remained on both fracture surfaces. However, the presence of C-O peaks (~285.5 eV), N1s peaks, and O1s peaks on the fracture surfaces also showed that the fracture surface was either intermittently located at the PS-CFRP interface or was covered in places by a very thin layer of PS (so that the XPS detected the epoxy material below). The presence of thin PS layers on both fracture surfaces is necessary to ensure sufficient autohesion between the separated plies during repair. The high repair effectiveness observed in PS-interleaved specimens indicates that the shear failure occurred predominantly within the PS interleaf, rather than at the interface with epoxy matrix.

4.3 Static indentation tests

Fig. 8 shows the load-displacement curves from the indentation test of a typical PS-interleaved composite subjected to three damage-repair cycles. Table 2 shows the average initial stiffness (determined over the displacement range of 0.2-0.4 mm) and the force at the damage onset (determined as the load corresponding to 1% increase in compliance) for the pristine and repaired composites. The recovery of the initial stiffness and damage onset force after three damage-repair cycles are 83.8% and 69.7% respectively, and there is very little change for successive repair cycles. However, it should be noted that there are significant variations in initial stiffness and damage onset force recovery, as shown by the standard deviation listed in Table 2 (but variability did not change significantly between the three repair cycles).

C-scan images included in Fig. 8 confirm that an approximately circular damage region of approximately 18 mm diameter was consistently achieved in the indentation tests of the pristine interleaved composites and subsequently repaired ones. After repair, the c-scan images still show some signs of damage in the indentation region, but the signal attenuation is greatly reduced.

Microscope examinations of the cross-section within the indentation region of as-manufactured composites, and after the 1st test and the 3rd repair cycle, were conducted (Fig. 9). The microscopic images show that no damage was observed within the composites as manufactured and confirm that interlaminar damage occurred after the 1st indentation. However, the images also show intralaminar failure of the interior composite plies in the indentation-damage zone. The intralaminar damage cannot be repaired using the ‘easy repair’ approach, and thus contributed to the reduction in stiffness and the damage onset force observed during tests of repaired specimens. The microscope image after the third test, shown in Fig. 9c, also indicates significant voids present in the PS interleaves. Void formation has been observed previously and was attributed to outgassing of PS [48] but is likely aggravated by PS loss during repair at elevated temperatures and pressure in combination with thermal relaxation resulting in shrinkage of the constricted PS film, which was stretched during extrusion in the production direction.

5 Conclusions

We proposed incorporating a 'weak link' thermoplastic interleaf within a thermoset composite to localise shear damage within the thermoplastic interleaf, so that this damage can subsequently be repaired readily by subjecting the composite to heat and pressure. In three-point bending tests of PS-interleaved composites, shear damage preferentially developed in the interleaf region. After repair, the stiffness was fully restored, and excellent recovery of the shear strength was achieved (88% of the pristine strength after two damage repair cycles) and so confirmed the easy repair capability of this weak-link strategy. In static indentation tests of the PS-interleaved composite panels, a good stiffness recovery of 84% was observed, but the damage onset force recovery was lower at around 70% after three damage repair cycles. The stiffness and damage onset force were quite constant during repeated damage-repair cycles. The incomplete recovery of stiffness and strength is due to the presence of intralaminar damage, which can not be repaired using the interleaf concept.

The PS-interleaved composite tests reported show that the 'weak link' concept is a very promising approach to achieving efficient repair of shear-driven interlaminar damage, a critical issue for composite structure longevity. To fully realise the strategy's potential, future work will investigate alternative interleaf materials with shear properties optimised to ensure that the interlaminar shear strength of the interleaved composites is not significantly lower than that of the parent composites, and with no void generation or interleaf material losses during repair. Future work will also consider the optimal thickness and location of the interleaf material, and investigate fully mechanical, thermal, creep and fatigue performance of interleaved composites. The evaluation of the 'weak link' strategy will be extended to other situations where interlaminar damage represents a significant failure risk, including low-velocity impact, stiffener run-out, stiffener pull-off and ply drops.

Acknowledgements

We acknowledge the help provided by Gary Senior, Jonathan Cole, Wiktor Piwowarczyk, and Keith Wolstenholme (Department of Aeronautics, Imperial College London) to manufacture and characterise test specimens, and Dr Andreas Mautner (Polymer & Composites Engineering Group, University of Vienna) for XPS measurements. We also acknowledge the funding from the European Union's Horizon 2020 research and innovation programme under the Marie Skłodowska-Curie scheme (No. 765881) within the framework of the HyFiSyn project.

CRediT

Bohao Zhang: Conceptualization, Formal analysis, Investigation, Methodology, Writing – original draft, Writing – review and editing. Gokul G. Murali: Investigation, Formal analysis, Writing – review and editing. Tomás Francisco Hut Quitéria: Investigation. Jakub Porzycki: Investigation. Yibo Bai: Investigation. Daniel Liew: Investigation. Tianyou Deng: Investigation. Chun Hei Yu: Investigation. Sameer Kanneganti: Investigation. Christroph Burgstaller: Resources, Investigation, Writing – review and editing. Alexander Bismarck: Conceptualization, Formal analysis, Funding acquisition, Methodology, Resources, Supervision, Writing – review and editing. Paul Robinson: Conceptualization, Formal analysis, Funding acquisition, Methodology, Resources, Supervision, Writing – review and editing.

Figures

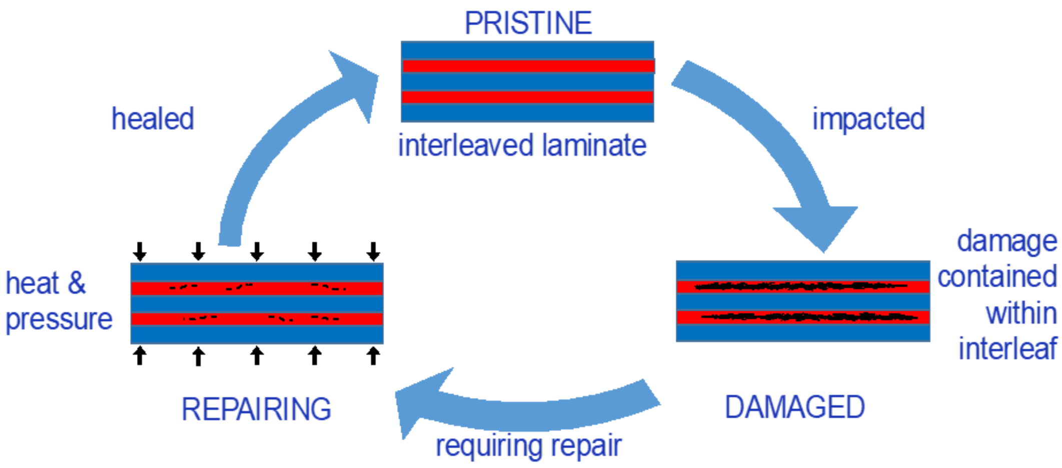

Fig. 1. Schematic of the damage-repair process of an interleaved composite.

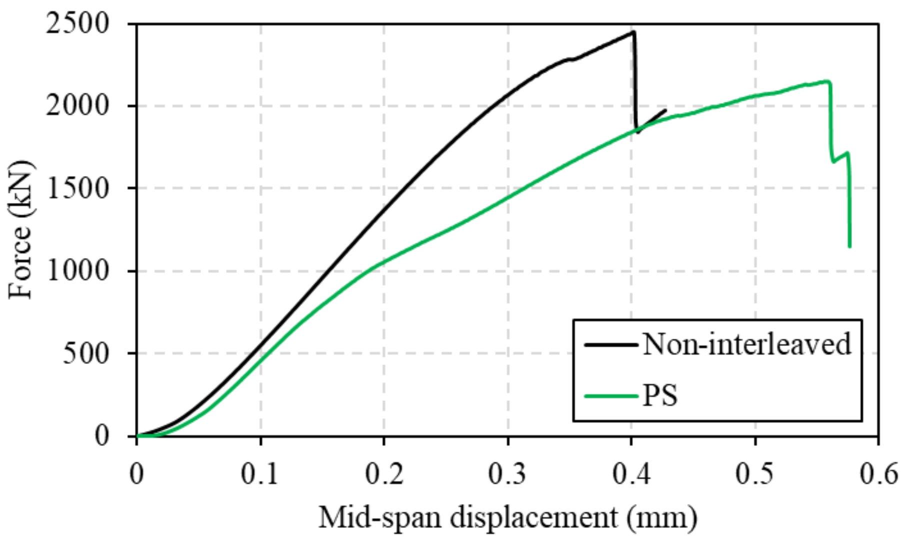

Fig. 2. Typical load-displacement curves from short beam shear tests.

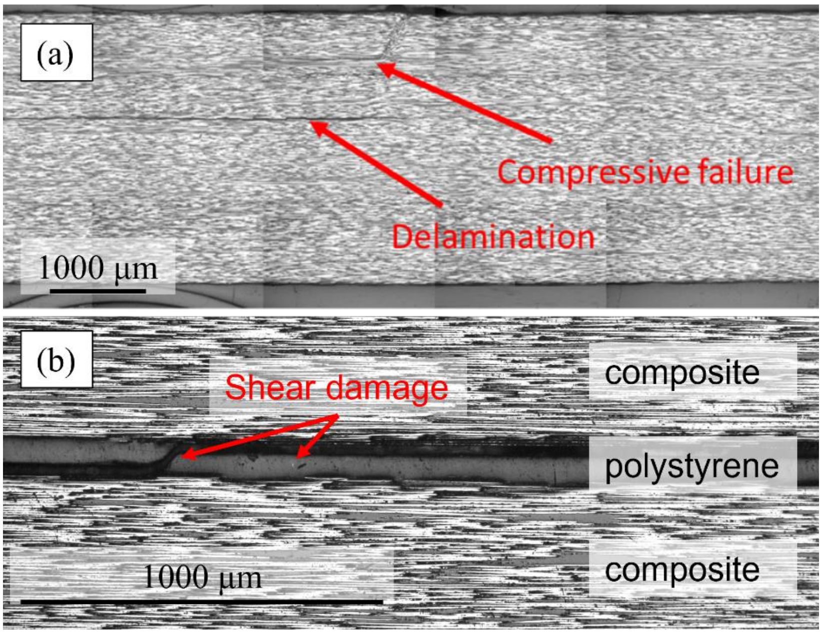

Fig. 3. Microscope images of the polished cross-sections after short beam shear test of (a) a non-interleaved specimen with initial delamination damage and subsequent compressive failure after further loading and (b) a PS-interleaved specimen with shear damage within the PS layer.

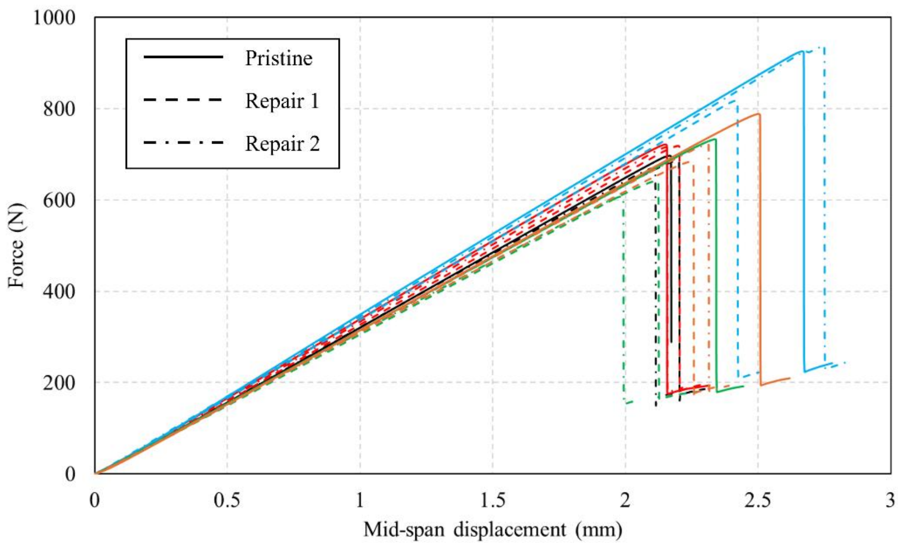

Fig. 4. The load-displacement curves from three-point bending test of a typical PS-interleaved composite specimen at different damage-repair cycles. Different colours are used for individual specimens.

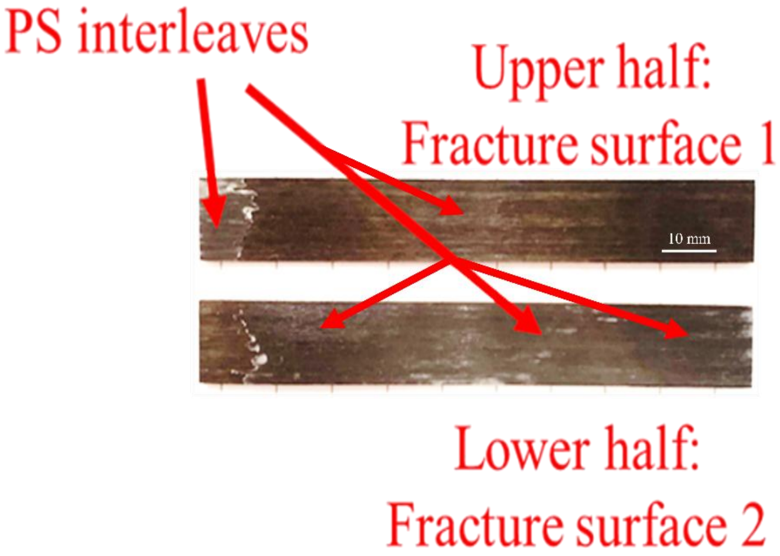

Fig. 5. Images of fracture surfaces of a PS-interleaved composite specimen.

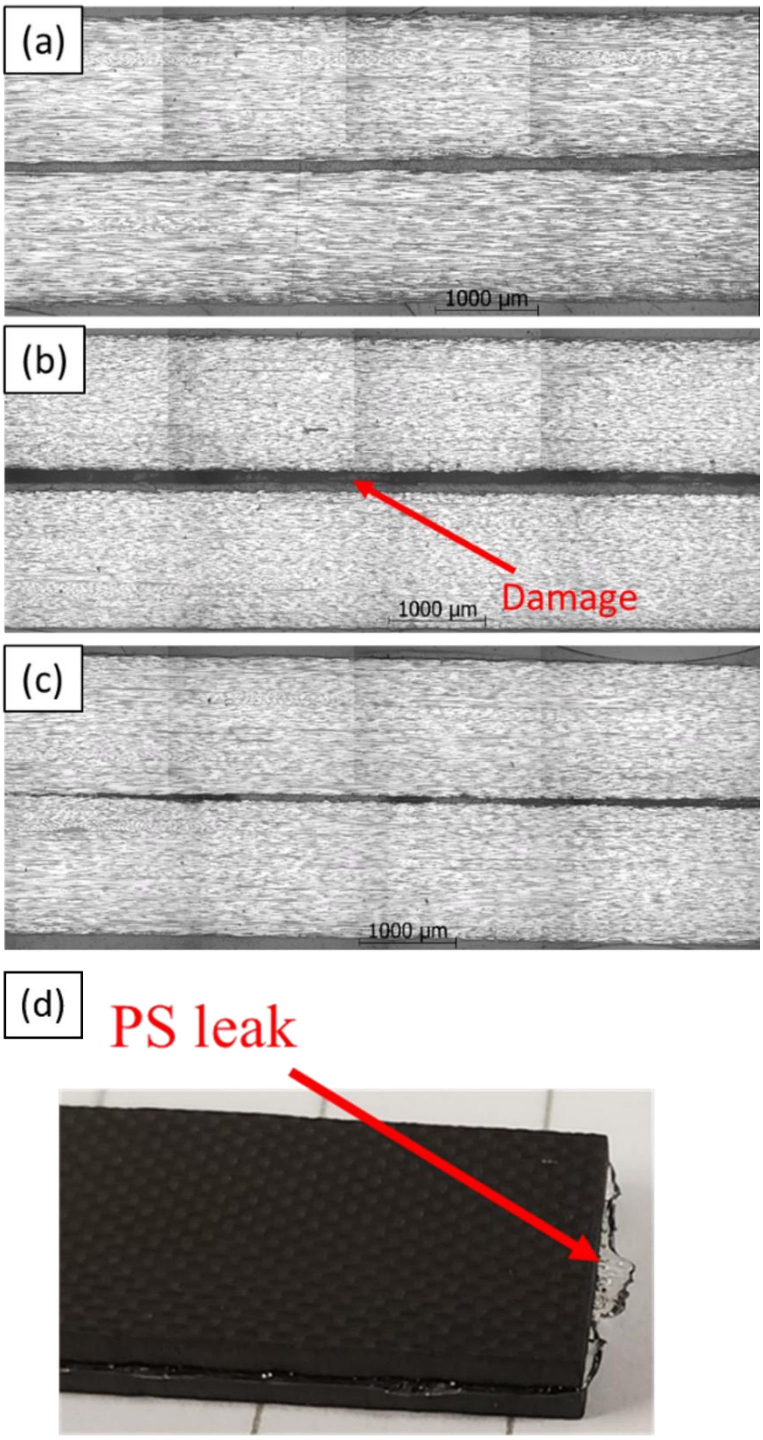

Fig. 6. (a-c) Microscope images of the cross-sections of PS-interleaved composites after manufacture, after the second bending test and after the second repair, and (d) PS leakage after a repair.

Specimen		Carbon peak (C1S)	Oxygen (O1S) and Nitrogen (N1S) peaks
Non-interleaved		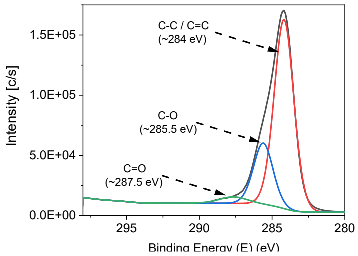	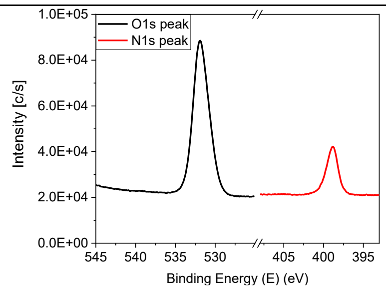
PS film		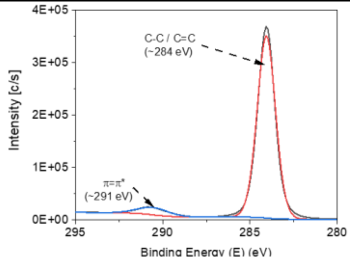	-
PS-interleaved	Fracture surface 1	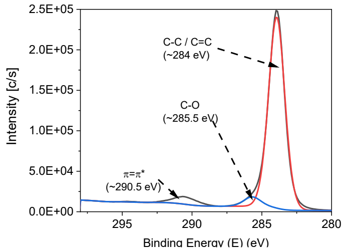	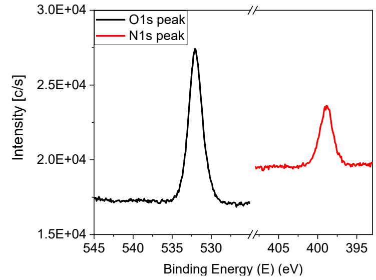
	Fracture surface 2	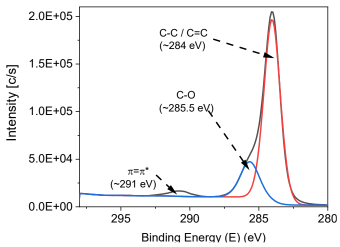	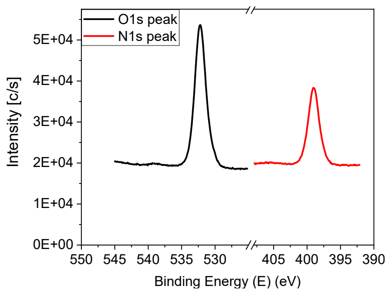

Fig. 7. The carbon (C1S), oxygen (O1S) and nitrogen (N1S) peaks of the XP-spectra of the surface of a non-interleaved composite specimen, PS film and the fracture surfaces of a PS-interleaved composite flexure test specimen.

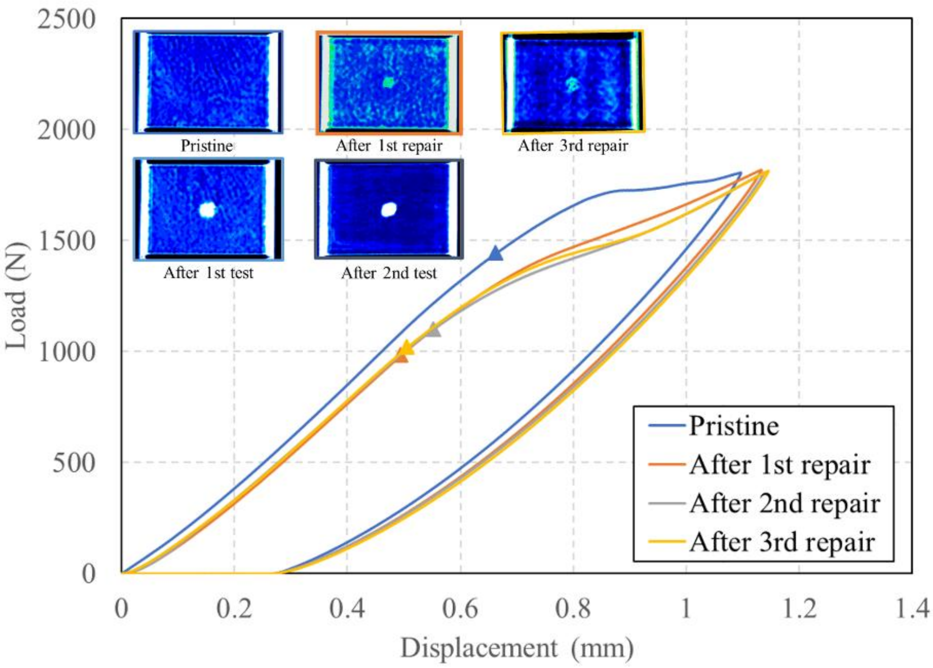

Fig. 8. The load-displacement curves from static indentation tests of a typical PS-interleaved composite specimen at three damage-repair cycles. The triangle symbols indicate the ‘damage onset’ force determined using the method in section 3.5.

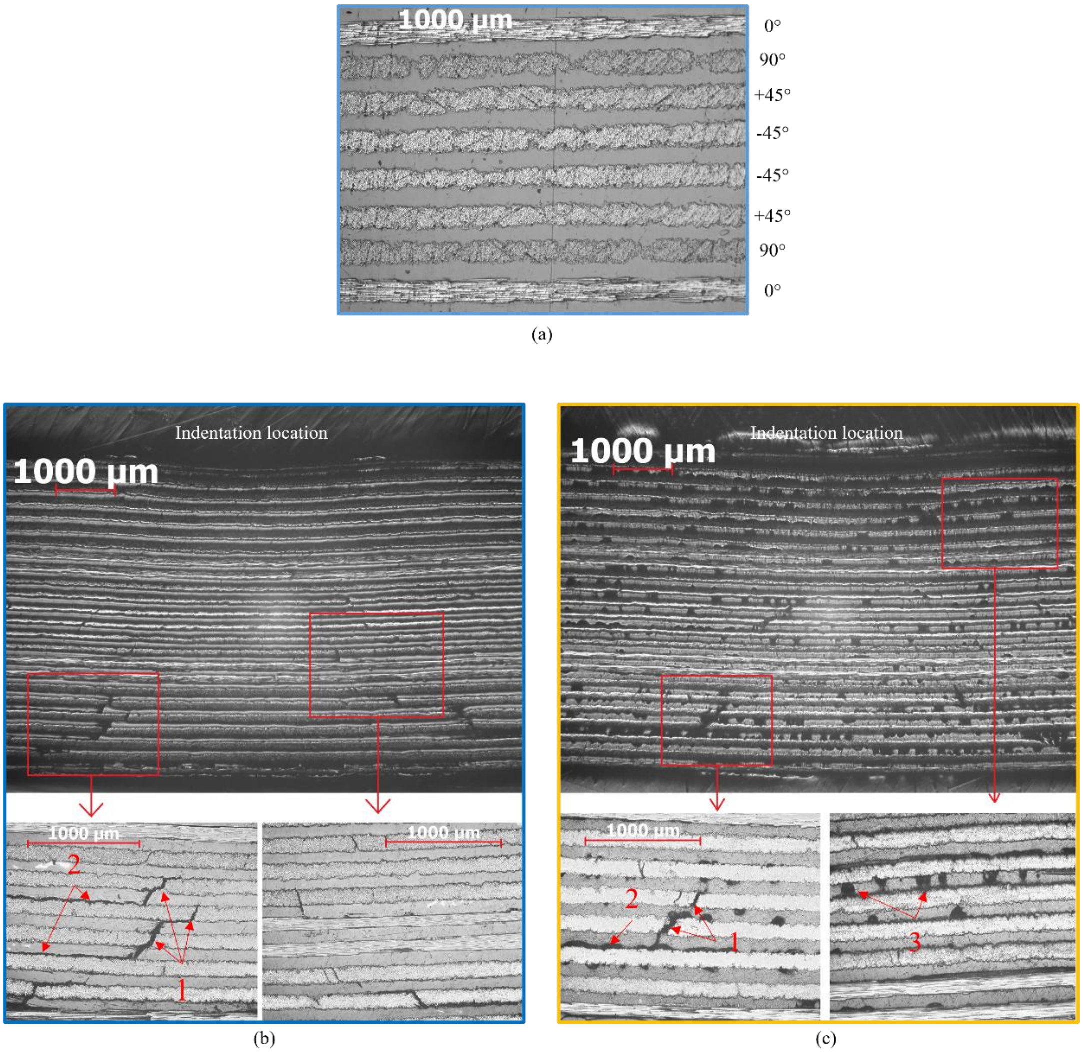

Fig. 9. (a) As-manufactured static indentation test panel (not at the full panel thickness), (b) after 1st test and (c) after 3rd test. (noted that '1' – interior composite ply fracture, '2' – delamination and '3' – voids)

Tables

Table 1. Dimensions of composite specimens subjected to short beam shear and three-point bending tests.

Specimen	Short beam shear tests			Three-point bending tests		
	length (mm)	width (mm)	thickness (mm)	length (mm)	width (mm)	thickness (mm)
Non-interleaved	15.18 (0.13)	6.17 (0.06)	2.90 (0.02)	-	-	-
PS-interleaved	15.82 (0.04)	5.88 (0.08)	2.95 (0.04)	80.75 (0.07)	9.93 (0.18)	2.85 (0.06)

Table 2. The average properties measured from short beam shear, three-point bending and static indentation tests of PS-interleaved composite specimens (standard deviation is shown in brackets).

Test method	Specimen	Property	Pristine	After 1st repair	Average recovery[1] (%)	After 2nd repair	Average recovery (%)	After 3rd repair	Average recovery (%)
Short beam shear	Non-interleaved	ILSS (MPa)	67.5 (1.7)	-	-	-	-	-	-
	PS-interleaved		31.3 (1.6)	-	-	-	-	-	-
Three-point bending	PS-interleaved	Interlaminar shear strength (MPa)	27.3 (1.2)	24.2 (0.5)	88.9 (3.7)	23.9 (1.2)	87.9 (6.2)	-	-
Static indentation	PS-interleaved	Initial stiffness (N/mm)	2432.0 (50.5)	2061.8 (219.8)	84.8 (9.2)	2030.4 (242.2)	83.5 (9.7)	2039.4 (241.4)	83.8 (9.8)
		Damage onset force (N)	1413.7 (113.4)	980.8 (205.0)	69.4 (12.9)	971.2 (177.7)	68.6 (10.6)	989.5 (201.1)	69.7 (11.1)

[1]recovery (%) = $\frac{\text{value after repair}}{\text{pristine value}} \times 100$

Table 3. Elemental composition from XPS analyses of non-interleaved composite, PS film and PS-interleaved composite specimens.

Sample description		Carbon (C1s) composition (%)	Oxygen (O1s) composition (%)	Nitrogen (N1s) composition (%)
Non-interleaved		79.41	15	5.59
PS film		100	0	0
PS-interleaved	Fracture surface 1	86.23	7.56	6.21
	Fracture surface 2	96.02	2.53	1.45

References

[1] M. Sohn, X. Hu, J.K. Kim, L. Walker, (2000) Impact damage characterisation of carbon fibre/epoxy composites with multi-layer reinforcement, *Composites Part B: Engineering*, **31** (8) pp 681-691 (https://doi.org/10.1016/S1359-8368(00)00028-7).

[2] A. Baker, (1984) Repair of cracked or defective metallic aircraft components with advanced fibre composites—an overview of Australian work, *Composite Structures*, **2** (2) pp 153-181 (https://doi.org/10.1016/0263-8223(84)90025-4).

[3] W. Zhou, X.-l. Ji, S. Yang, J. Liu, L.-h. Ma, (2021) Review on the performance improvements and non-destructive testing of patches repaired composites, *Composite Structures*, **263** pp 113659 (https://doi.org/10.1016/j.compstruct.2021.113659).

[4] M. Lena, J. Klug, C. Sun, (1998) Composite patches as reinforcements and crack arrestors in aircraft structures, *Journal of Aircraft*, **35** (2) pp 318-323 (https://doi.org/10.2514/2.2302).

[5] V.S. Balakrishnan, H. Seidlitz, (2018) Potential repair techniques for automotive composites: A review, *Composites Part B: Engineering*, **145** pp 28-38 (https://doi.org/10.1016/j.compositesb.2018.03.016).

[6] M. Thunga, A. Bauer, K. Obusek, R. Meilunas, M. Akinc, M.R. Kessler, (2014) Injection repair of carbon fiber/bismaleimide composite panels with bisphenol E cyanate ester resin, *Composites Science and Technology*, **100** pp 174-181 (https://doi.org/10.1016/j.compscitech.2014.05.024).

[7] M. Thunga, K. Larson, W. Lio, T. Weerasekera, M. Akinc, M.R. Kessler, (2013) Low viscosity cyanate ester resin for the injection repair of hole-edge delaminations in bismaleimide/carbon fiber composites, *Composites Part A: Applied Science and Manufacturing*, **52** pp 31-37 (https://doi.org/10.1016/j.compositesa.2013.05.001).

[8] B.J. Blaiszik, S.L. Kramer, S.C. Olugebefola, J.S. Moore, N.R. Sottos, S.R. White, (2010) Self-healing polymers and composites, *Annual review of materials research*, **40** (1) pp 179-211 (https://doi.org/10.1146/annurev-matsci-070909-104532).

[9] Y. Wang, D.T. Pham, C. Ji, (2015) Self-healing composites: A review, *Cogent Engineering*, **2** (1) pp 1075686 (https://doi.org/10.1080/23311916.2015.1075686).

[10] S. Ilyaei, R. Sourki, Y.H.A. Akbari, (2021) Capsule-based healing systems in composite materials: A review, *Critical Reviews in Solid State and Materials Sciences*, **46** (6) pp 491-531 (https://doi.org/10.1080/10408436.2020.1852912).

[11] M. Kessler, N.R. Sottos, S. White, (2003) Self-healing structural composite materials, *Composites Part A: Applied Science and Manufacturing*, **34** (8) pp 743-753 (https://doi.org/10.1016/S1359-835X(03)00138-6).

[12] J.L. Moll, S.R. White, N.R. Sottos, (2010) A self-sealing fiber-reinforced composite, *Journal of composite materials*, **44** (22) pp 2573-2585 (https://doi.org/10.1177/0021998309356605).

[13] A.J. Patel, N.R. Sottos, E.D. Wetzel, S.R. White, (2010) Autonomic healing of low-velocity impact damage in fiber-reinforced composites, *Composites Part A: Applied Science and Manufacturing*, **41** (3) pp 360-368 (https://doi.org/10.1016/j.compositesa.2009.11.002).

[14] K. Sanada, I. Yasuda, Y. Shindo, (2006) Transverse tensile strength of unidirectional fibre-reinforced polymers and self-healing of interfacial debonding, *Plastics, rubber and composites*, **35** (2) pp 67-72 (https://doi.org/10.1179/174328906X79914).

[15] S.R. White, N.R. Sottos, P.H. Geubelle, J.S. Moore, M.R. Kessler, S. Sriram, E.N. Brown, S. Viswanathan, (2001) Autonomic healing of polymer composites, *Nature*, **409** (6822) pp 794-797 (https://doi.org/10.1038/35057232).

[16] B. Blaiszik, N. Sottos, S. White, (2008) Nanocapsules for self-healing materials, *Composites Science and Technology*, **68** (3-4) pp 978-986 (https://doi.org/10.1016/j.compscitech.2007.07.021).
[17] M. Kosarli, D.G. Bekas, K. Tsirka, D. Baltzis, D.T. Vaimakis-Tsogkas, S. Orfanidis, G. Papavassiliou, A.S. Paipetis, (2019) Microcapsule-based self-healing materials: Healing efficiency and toughness reduction vs. capsule size, *Composites Part B: Engineering*, **171** pp 78-86 (https://doi.org/10.1016/j.compositesb.2019.04.030).
[18] S. Bleay, C. Loader, V. Hawyes, L. Humberstone, P. Curtis, (2001) A smart repair system for polymer matrix composites, *Composites Part A: Applied Science and Manufacturing*, **32** (12) pp 1767-1776 (https://doi.org/10.1016/S1359-835X(01)00020-3).
[19] M.D. Hager, P. Greil, C. Leyens, S. Van Der Zwaag, U.S. Schubert, (2010) Self-healing materials, *Advanced Materials*, **22** (47) pp 5424-5430 (https://doi.org/10.1002/adma.201003036).
[20] K.R. Hart, S.M. Lankford, I.A. Freund, J.F. Patrick, B.P. Krull, E.D. Wetzel, N.R. Sottos, S.R. White, (2017) Repeated healing of delamination damage in vascular composites by pressurized delivery of reactive agents, *Composites Science and Technology*, **151** pp 1-9 (https://doi.org/10.1016/j.compscitech.2017.07.027).
[21] I.L. Hia, V. Vahedi, P. Pasbakhsh, (2016) Self-healing polymer composites: prospects, challenges, and applications, *Polymer Reviews*, **56** (2) pp 225-261 (https://doi.org/10.1080/15583724.2015.1106555).
[22] J.W. Pang, I.P. Bond, (2005) A hollow fibre reinforced polymer composite encompassing self-healing and enhanced damage visibility, *Composites Science and Technology*, **65** (11-12) pp 1791-1799 (https://doi.org/10.1016/j.compscitech.2005.03.008).
[23] D. Therriault, S.R. White, J.A. Lewis, (2003) Chaotic mixing in three-dimensional microvascular networks fabricated by direct-write assembly, *Nature materials*, **2** (4) pp 265-271 (https://doi.org/10.1038/nmat863).
[24] K.S. Toohey, N.R. Sottos, J.A. Lewis, J.S. Moore, S.R. White, (2007) Self-healing materials with microvascular networks, *Nature materials*, **6** (8) pp 581-585 (https://doi.org/10.1038/nmat1934).
[25] G. Williams, R. Trask, I. Bond, (2007) A self-healing carbon fibre reinforced polymer for aerospace applications, *Composites Part A: Applied Science and Manufacturing*, **38** (6) pp 1525-1532 (https://doi.org/10.1016/j.compositesa.2007.01.013).
[26] H.R. Williams, R. Trask, I. Bond, (2007) Self-healing composite sandwich structures, *Smart Materials and Structures*, **16** (4) pp 1198 (10.1088/0964-1726/16/4/031).
[27] H.R. Williams, R.S. Trask, I. Bond, (2008) Self-healing sandwich panels: restoration of compressive strength after impact, *Composites Science and Technology*, **68** (15-16) pp 3171-3177 (https://doi.org/10.1016/j.compscitech.2008.07.016).
[28] X. Chen, M.A. Dam, K. Ono, A. Mal, H. Shen, S.R. Nutt, K. Sheran, F. Wudl, (2002) A thermally re-mendable cross-linked polymeric material, *Science*, **295** (5560) pp 1698-1702 (https://doi.org/10.1126/science.1065879).
[29] X. Chen, F. Wudl, A.K. Mal, H. Shen, S.R. Nutt, (2003) New thermally remendable highly cross-linked polymeric materials, *Macromolecules*, **36** (6) pp 1802-1807 (https://doi.org/10.1021/ma0210675).
[30] S. Hayes, F. Jones, K. Marshiya, W. Zhang, (2007) A self-healing thermosetting composite material, *Composites Part A: Applied Science and Manufacturing*, **38** (4) pp 1116-1120 (https://doi.org/10.1016/j.compositesa.2006.06.008).

[31] S.A. Hayes, W. Zhang, M. Branthwaite, F. Jones, (2007) Self-healing of damage in fibre-reinforced polymer-matrix composites, *Journal of the Royal Society Interface*, **4** (13) pp 381-387 (https://doi.org/10.1098/rsif.2006.0209).

[32] K. Pingkarawat, C. Wang, R. Varley, A. Mouritz, (2012) Self-healing of delamination fatigue cracks in carbon fibre–epoxy laminate using mendable thermoplastic, *Journal of Materials Science*, **47** pp 4449-4456 (https://doi.org/10.1007/s10853-012-6303-8).

[33] K. Pingkarawat, C. Wang, R. Varley, A. Mouritz, (2012) Self-healing of delamination cracks in mendable epoxy matrix laminates using poly [ethylene-co-(methacrylic acid)] thermoplastic, *Composites Part A: Applied Science and Manufacturing*, **43** (8) pp 1301-1307 (https://doi.org/10.1016/j.compositesa.2012.03.010).

[34] A. Cohades, E. Manfredi, C.J. Plummer, V. Michaud, (2016) Thermal mending in immiscible poly (ε-caprolactone)/epoxy blends, *European Polymer Journal*, **81** pp 114-128 (https://doi.org/10.1016/j.eurpolymj.2016.05.026).

[35] A. Cohades, V. Michaud, (2017) Thermal mending in E-glass reinforced poly (ε-caprolactone)/epoxy blends, *Composites Part A: Applied Science and Manufacturing*, **99** pp 129-138 (https://doi.org/10.1016/j.compositesa.2017.04.013).

[36] A. Kandemir, M.L. Longana, I. Hamerton, S.J. Eichhorn, (2022) Developing aligned discontinuous flax fibre composites: Sustainable matrix selection and repair performance of vitrimers, *Composites Part B: Engineering*, **243** pp 110139 (https://doi.org/10.1016/j.compositesb.2022.110139).

[37] D.R. Palubiski, M.L. Longana, J.M. Dulieu-Barton, I. Hamerton, D.S. Ivanov, (2023) Multi-matrix continuously-reinforced composites: A novel route to sustainable repair of composite structures, *Materials & Design*, **235** pp 112446 (https://doi.org/10.1016/j.matdes.2023.112446).

[38] O. Ishai, H. Rosenthal, N. Sela, E. Drukker, (1988) Effect of selective adhesive interleaving on interlaminar fracture toughness of graphite/epoxy composite laminates, *Composites*, **19** (1) pp 49-54 (https://doi.org/10.1016/0010-4361(88)90543-5).

[39] D.W. Wong, L. Lin, P.T. McGrail, T. Peijs, P.J. Hogg, (2010) Improved fracture toughness of carbon fibre/epoxy composite laminates using dissolvable thermoplastic fibres, *Composites Part A: Applied Science and Manufacturing*, **41** (6) pp 759-767 (https://doi.org/10.1016/j.compositesa.2010.02.008).

[40] S. Chen, B. Jang, (1991) Fracture behaviour of interleaved fiber-resin composites, *Composites Science and Technology*, **41** (1) pp 77-97 (https://doi.org/10.1016/0266-3538(91)90054-S).

[41] W. Lu, F. Liao, A. Su, P. Kao, T. Hsu, (1995) Effect of interleaving on the impact response of a unidirectional carbon/epoxy composite, *Composites*, **26** (3) pp 215-222 (https://doi.org/10.1016/0010-4361(95)91385-I).

[42] T.D. Thorn, Y. Liu, X. Yao, D.G. Papageorgiou, P. Robinson, E. Bilotti, T. Peijs, H. Zhang, (2023) Smart and repeatable easy-repairing and self-sensing composites with enhanced mechanical performance for extended components life, *Composites Part A: Applied Science and Manufacturing*, **165** pp 107337 (https://doi.org/10.1016/j.compositesa.2022.107337).

[43] T.D. Thorn, Y. Wang, H. Guo, L. Lu, Y. Liu, E. Bilotti, D.G. Papageorgiou, H. Zhang, (2024) Discontinuous interleaving strategies for toughening, damage sensing and repair in multifunctional carbon fibre/epoxy composites, *Composites Part A: Applied Science and Manufacturing*, **185** pp 108320 (https://doi.org/10.1016/j.compositesa.2024.108320).

[44] Q. OuYang, X. Wang, L. Liu, (2022) High crack self-healing efficiency and enhanced free-edge delamination resistance of carbon fibrous composites with hierarchical

interleaves, *Composites Science and Technology*, **217** pp 109115 (https://doi.org/10.1016/j.compscitech.2021.109115).
[45] P. Robinson, B. Zhang, S. Kanneganti, A. Bismarck, H. Maples, C. Burgstaller, EASY REPAIR OF INTERLAMINAR DAMAGE USING INTERLEAVED CARBON FIBRE/EPOXY COMPOSITES, International Conference on Composite Materials, Xi'an, China, 2017.
[46] Hexcell, Fibredux 914 High temperature resistance unidirectional prepregs, Cambridge, 1989.
[47] H.A. Maples, S. Wakefield, P. Robinson, A. Bismarck, (2014) High performance carbon fibre reinforced epoxy composites with controllable stiffness, *Composites Science and Technology*, **105** pp 134-143
[48] P. Robinson, A. Bismarck, B. Zhang, H.A. Maples, (2017) Deployable, shape memory carbon fibre composites without shape memory constituents, *Composites Science and Technology*, **145** pp 96-104 (https://doi.org/10.1016/j.compscitech.2017.02.024).
[49] H. Cui, S. Koussios, Y. Li, A. Beukers, (2013) Measurement of adhesive shear properties by short beam shear test based on higher order beam theory, *International journal of adhesion and adhesives*, **40** pp 19-30 (https://doi.org/10.1016/j.ijadhadh.2012.08.009).
[50] ASTM D2344/D2344M-22 Standard Test Method for Short-Beam Strength of Polymer Matrix Composite Materials and Their Laminates, ASTM D2344/D2344M-22, ASTM International, United States, 2022.
[51] W. Cui, M.R. Wisnom, M. Jones, (1994) Effect of specimen size on interlaminar shear strength of unidirectional carbon fibre-epoxy, *Composites engineering*, **4** (3) pp 299-307 (https://doi.org/10.1016/0961-9526(94)90080-9).
[52] G.B. Beamson, D., High Resolution XPS of Organic Polymers: The Scienta ESCA300 Database, New York, 1992.

Easy repair enabled by an interleaving 'weak link' strategy to localise damage in laminated fibre-reinforced polymer-matrix composites

Bohao Zhang[1], Gokul G. Murali[1], Tomás Francisco Hut Quitéria[1], Jakub Porzycki[1], Yibo Bai[1], Daniel Liew[1], Tianyou Deng[1], Chun Hei Yu[1], Sameer Kanneganti[1], Christroph Burgstaller[2], Alexander Bismarck[3,4] and Paul Robinson[†*]

Supplementary material

S.1 Experimental investigation of PLA and ASA+PC interleaved composite specimens

S.1.1 Materials

Short beam shear and 3-point bending tests were also performed on composites containing a mid-plane interleaf of two other materials. These were polylactic acid (PLA) (IngeoTM 2003D) and a poly (acrylonitrile styrene acrylate)/polycarbonate (ASA+PC) blend (Luran S KR2863C). In particular, ASA+PC interleaved composites were investigated because the higher polarity of this interleaf material (due to the presence of nitrile groups), compared to PS, may result in better adhesion to the epoxy matrix. This, together with the higher intrinsic strength of ASA+PC, was expected to improve the shear strength of the interleaved composite.

Rolls of thin sheets of PLA (100 μm thick) and ASA+PC (100 μm thick) were produced supplied by Transfercenter für Kunststofftechnik (TCKT, Austria).

S.1.2 Repair process

The PLA-interleaved 3-point bend specimens failed in the interleaf region and debonded into two halves along the thickness. These were repaired in the same manner as described in section 3.7 at 190°C, as this is the melting temperature of the PLA interleaf.

The ASA+PC bending test specimens did not fail in the interleaf region and so no repair was performed.

S.1.3 Short beam shear tests

Fig. S1 shows the typical load-displacement plots of a PLA and a ASA+PC specimen respectively. The PLA-interleaved specimen demonstrated an almost linear relationship, after some initial ‘bedding in’, with a sharp drop at around 700 N. The ASA+PC-interleaved specimen showed an initially linear response (after ‘bedding in’) but then showed a softening behaviour. To determine the ILSS for the PLA-interleaved specimen, the maximum load at the first load drop was used. For the ASA+PC-interleaved specimens the load at 1% compliance increase was used. The initial stiffness was measured within the mid-span displacement range of 0.15-0.20 mm.

The average ILSS associated with the failure of the PLA-interleaved specimens was 26.7 MPa (see Table S1). This is significantly lower than the ILSS of the non-interleaved composite and confirms that the PLA interleaf has introduced a 'weak link' into the composite studied here. For the composite material used in this investigation, the transition to shear failure in the three-point bending test is predicted to occur when the shear strength of the interleaved specimen is less than approximately 29 MPa. (This can be readily calculated using the flexural strength of the non-interleaved composite together with the span and the thickness of the interleaved specimens.) The measured ILSS therefore suggests that the three-point bending test of the PLA-interleaved specimen will fail in shear. However, as mentioned, the short beam shear test is widely regarded as a qualitative rather than a quantitative method [50, 51].

As shown in Fig. S1, yielding of an ASA+PC-interleaved specimen initiated at around 1350 N and ultimate failure occurred at around 2000 N. The ILSS, associated with the onset of the failure, was 59.8 MPa (see Table S1), which is much higher than the shear failure transition value and so shear failure is not expected in the 3-point bending test of these interleaved composites.

S.1.4 Three-point bending tests

Typical load-displacement curves recorded in the three-point bending test in the pristine state and after the first and second repair (see Fig. S2(a)) of a PLA-interleaved specimen show that the stiffness of the specimen was almost unchanged after each repair. The corresponding shear strengths were 10.7 MPa after the first flexure test (i.e. in the pristine state), 4.6 MPa after the first repair (43% of pristine value) and 4.7 MPa after the second repair (44% of the pristine value), as shown in Table S1. Average fracture stress from short-beam shear and three-point bending tests of PLA and ASA+PC specimens. (The shear strength τ^u of the pristine specimen determined using the three-point bending tests is much smaller than the ILSS determined by the short beam shear tests; this is attributed to the inaccuracy of equation (1) for the short beam shear configuration [49].) All specimens failed by shear resulting in separation in the interleaf region. Microscope examination shows that a distinct continuous PLA interleaf can be seen in the mid-plane of the composites in polished cross-sections of the pristine flexure specimens (Fig. S3(a)). After the first test, failure appears to occur at the PLA/composite interface (Fig. S3(b)) and after repair (Fig. S3(c)) the PLA seems to have re-bonded to the composite plies but some cracks can still be seen in the PLA/composite interface. Also, some leakage of PLA during the repair process was observed in a few specimens due to the applied pressure. The poor repair effectiveness of these interleaved specimens is most probably because the PLA does not re-bond well to the cured epoxy and because of the loss of PLA during a repair. Upon XPS characterisation, PLA films have a higher C=O (~289 eV) / C-C (~284 eV) peak intensity ratio compared to non-interleaved composites (Fig. S4). The deconvoluted high-resolution C1s peaks of PLA are similar to the results reported previously [52]. On both the fracture surfaces of PLA-interleaved composites (see Fig. S4), the C=O peaks (~288 eV) and N1s peaks indicated the presence of both PLA and CFRP. This confirmed the presence of an intermittent or a very thin PLA layer on both fracture surfaces. The relatively poor repair efficiencies recorded for the PLA suggests that shear failure occurred predominantly at the interface with the composite ply and that this interface was weak after repair. (This was in contrast to the PS interleaf described in the main paper.)

The typical load-displacement curve of an ASA+PC–interleaved specimen subjected to three-point bending test is shown in Fig. S2(b). As expected, these specimens did not fail in shear. Failure was due to compression at the upper surface, and the average flexural strength was measured to be 1229 MPa (see Table S1). No damage was observed within the ASA+PC layer or at the interleaf/composite interface and so no repairs were performed of this interleaved configuration.

S.1.5 Summary

The PLA-interleaved composite was shown to be too weak in shear and its repair efficiency was low compared to the case of PS described in the main paper. Composite containing an ASA+PC interleaf was shown to have a higher ILSS value than the PS case but still low enough (in comparison to the ILSS value of the non-interleaved composite) to act as a weak link. The span of the 3-point bending configuration used here, was not sufficiently short to initiate shear failure and so no repair was performed. Shorter span tests should be used to evaluate the repair effectiveness of this interleaf material and, if successful, static indentation tests should be performed to establish practical applicability.

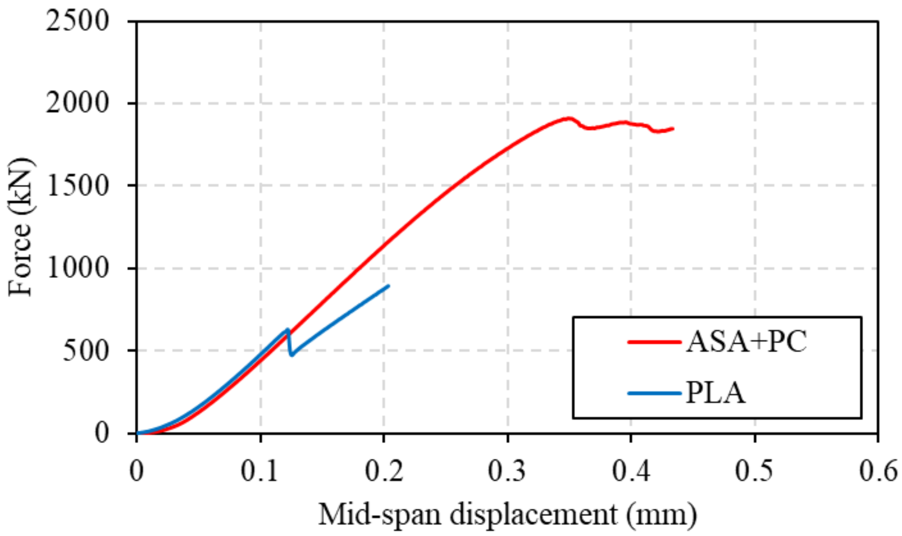

Fig. S1. Typical load-displacement curves from short beam shear tests

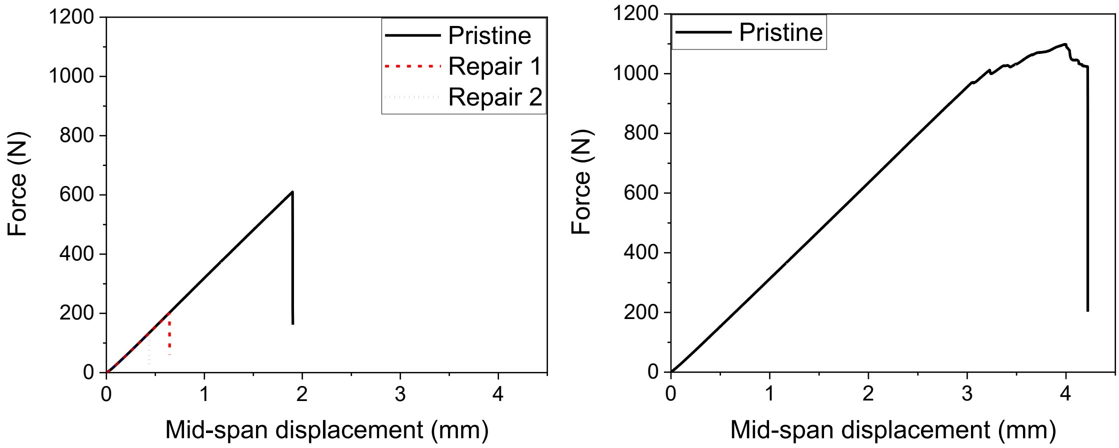

(a) (b)

Fig. S2. The load-displacement curves from three-point bending tests of a typical (a) PLA-interleaved specimen at different damage-repair cycles and (b) ASA+PC-interleaved composite specimen.

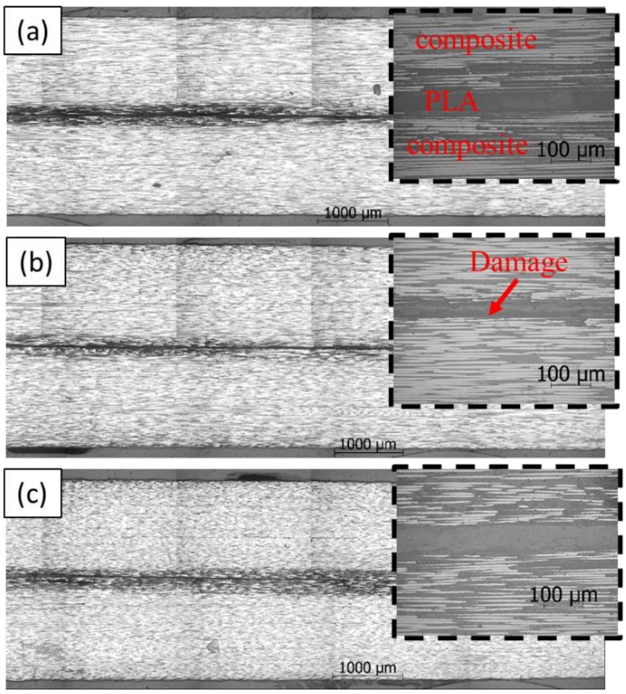

Fig. S3. Microscope images of the polished cross-sections of a PLA-interleaved composite subjected to three-point flexure test a) after manufacture, b) after test and c) after the second repair.

Sample description		Carbon peak (C1S)	Oxygen (O1S) and Nitrogen (N1S) peaks
Pristine PLA film		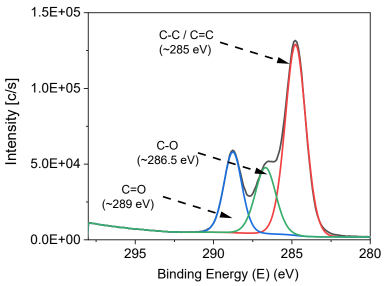	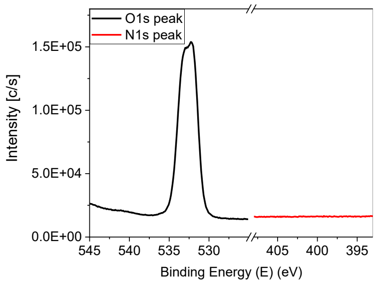
PLA-interleaved composite	Fracture surface 1	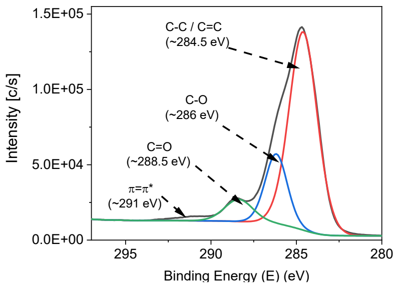	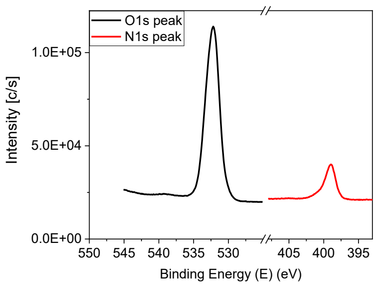
	Fracture surface 2	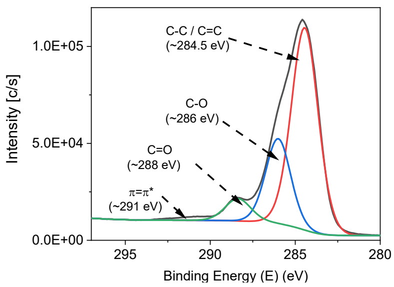	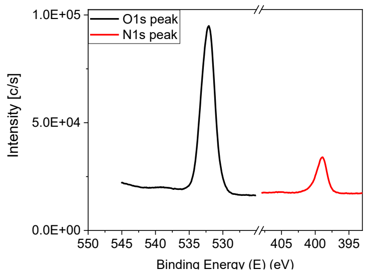

Fig. S4. The carbon (C1S), oxygen (O1S) and nitrogen (N1S) peaks of the XP-spectra of PLA film and both fracture surfaces of PLA-interleaved composites from three-point bending test.

Table S1. Average fracture stress from short-beam shear and three-point bending tests of PLA and ASA+PC specimens (standard deviation is shown in brackets).

Test method	Specimen	Property	Pristine	After 1st repair	Average recovery[1] (%)	After 2nd repair	Average recovery (%)

Short beam shear	PLA-interleaved	ILSS (MPa)	26.7 (3.1)	-	-	-	-
	ASA+PC-interleaved		59.8 (3.6)	-	-	-	-
Three-point bending	PLA-interleaved	Interlaminar shear strength (MPa)	10.7 (3.1)	4.6 (3.2)	43	4.7 (3.3)	44
	ASA+PC-interleaved		26.4 (1.4)	-	-	-	-

[1]recovery (%) = $\frac{\text{value after repair}}{\text{pristine value}} \times 100$